

Highly Efficient High-Power Rectenna with the Diode on Antenna (DoA) Topology

Kenji ITOH^{†a)}, Naoki SAKAI[†], and Keisuke NOGUCHI[†], Members

SUMMARY In this paper, a high-efficiency high-power rectenna with a bridge diode and the diode on antenna (DoA) topology is discussed. First, the topologies of rectifiers and rectennas are discussed to indicate the direction for obtaining highly efficient rectification. Rectifiers with well-matched diode pairs, as double voltage and bridge rectifiers, can reactively terminate even order harmonics, and is suitable for highly efficient operation. A rectenna with the DoA topology is suitable for a direct connection between the highly functional antenna and the rectifier diodes to remove lossy circuit portions. Next, the formulas for the rectification efficiency of the bridge rectifier are demonstrated with the behavioral model. The indicated formulas clarify the fundamental limitation on the rectification efficiency, which is the design goal in case of the DoA topology. Finally, we demonstrate a 5.8 GHz band 1 W rectenna with the bridge diode and the DoA topology. The bridge rectifier that is directly connected to the inductive high-impedance antenna achieved a rectification efficiency of 92.8% at an input power of 1 W. This is close to the fundamental limitation due to the diode performance.

key words: wireless power transfer, rectenna, rectifier, diode, antenna

1. Introduction

Wireless power transmission systems in microwaves (MPTs) have been studied since the 1960s for solar power satellite systems (SPS) [1]–[4]. In addition to SPS, MPT systems have been studied for unmanned aerial vehicles, such as drones and airships [5], [6]. High-power transmission technologies with high efficiency are required to expand the applications of MPT systems. At present, the “Internet of Things” era requires social implementations of “real wireless systems without power lines”.

In high-power MPT systems, the hardware bottleneck of the transfer efficiency is a rectenna with an antenna and a rectifier. Thus, a highly efficient rectenna is the key component. Antennas, circuits, and semiconductor techniques to improve efficiencies in 1 to 10 W-class rectifiers/rectenna have been studied for the above applications [1], [2], [4], [5].

In this paper, high-power rectifiers and rectennas are discussed for highly efficient MPT systems. The bridge rectifiers are focused, because of the advantage of high efficiencies with well-matched diode pairs. Our concentration on bridge rectifiers [7]–[11] is due to the previous research on diode mixers, such as even harmonic mixers [12] or ring mixers [13]. Even in millimeter-waves, mixers with well-matched diode pairs maintain their basic behaviors related

to the termination of harmonics. The bridge diode as a well-matched diode pair can realize the highly efficient rectification due to well even-order harmonics’ reaction. In the following discussions, we provide an overview of high-power rectifier/rectenna topologies and describe our work on the formulation of the rectification efficiency with the behavioral model and the implemented rectenna.

2. High Power Rectifier/Rectenna Topologies and the DoA Topology

Figure 1 shows the rectifier topologies in previous studies. The most common topology is the single-shunt rectifier, as shown in Fig. 1 (a) [1], [2], [5], [14]. This rectifier topology employs a harmonic reaction circuit for full-wave rectification with a single diode. In the 1970s, a 2.4 GHz band single shunt rectifier with a GaAs Schottky barrier diode (SBD) achieved a rectification efficiency of 90% at an input power of 8 W [14]. Double voltage rectifiers [15] and bridge rectifiers [7]–[11], [14] contain several rectifier diodes, as shown in Figs. 1 (b) and (c), respectively. Both rectifiers employ matched diodes for the reactive termination of even-order

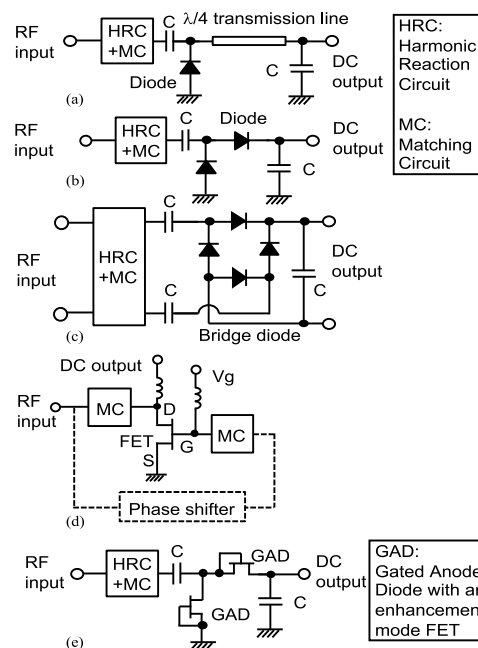


Fig. 1 Topologies of (a) a single shunt rectifier, (b) a double voltage rectifier, (c) a bridge rectifier, (d) a synchronous rectifier and (e) a gated anode diode rectifier [21].

Manuscript received January 30, 2022.

Manuscript publicized March 25, 2022.

[†]The authors are with Kanazawa Institute of Technology, Nonoichi-shi, 921–8501 Japan.

a) E-mail: itoh.kenji@neptune.kanazawa-it.ac.jp

DOI: 10.1587/transele.2022MMI0007

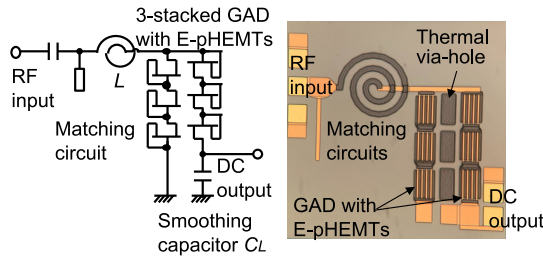


Fig. 2 5.8 GHz band double voltage rectifier MMIC with $0.5 \mu\text{m}$ E-PHEMT gated anode diode (GAD) [21].

harmonics. Thus, they are suitable for monolithic integration as they contain fewer circuit components than single-shunt rectifiers. In the 1960s, a 2.4 GHz band bridge rectifier for SPS applications was reported [14], after which there have been fewer reports on high-power rectification with bridge rectifiers. In the 2010s, we reported bridge rectifiers with a focus on their miniaturization and high-efficiency, because of well reactive termination on even-order harmonics [7]–[11]. Even today, bridge rectifiers are mainly applied to low-power utilizations for energy harvesting. However, a high-power bridge rectifier was reported in [16] in addition to our studies mentioned above. Figures 1 (d) and (e) indicate field effect transistor (FET) rectifier topologies, instead of diode rectifiers. As there are only a few commercial diodes used for high-power rectifications, synchronous rectifiers configured with an FET amplifier as a rectification device were proposed, as shown in Fig. 1 (d) [17], [18]. The topology enables high-power operation owing to the high current density of the FETs. Compared with diode rectifiers, the reported rectification efficiencies are relatively low because of the internal/external feedback mechanism for gate switching. Another FET rectifier topology is the gated anode diode (GAD) topology configured with the enhancement mode FET, as shown in Fig. 1 (e) [19]–[21]. The gate and drain electrodes of the FET are connected to configure the GAD that behaves as a diode. This is a common circuit technique for low-power CMOS rectifiers for radio-frequency identification (RFID) [19]. For high-power rectification, the higher current density of the FET compared to that of the SBD makes the same high-power performance as the reported synchronous rectifiers, and the same circuit topology as the diode rectifier results in highly efficient performance. For high-power rectification, we reported a SOI-CMOS bridge rectifier [20] and a GaAs enhancement mode pseudomorphic-HEMT (E-PHEMT) double-voltage rectifier [21]. The developed 5.8 GHz band GaAs rectifier MMIC shown in Fig. 2 achieved a rectification efficiency of 77.9% at an input power of 37.1 dBm, with a $0.5 \mu\text{m}$ GaAs E-PHEMT GAD. Furthermore, we reported a GaN HEMT GAD with a breakdown voltage of 40 V for 10 W class rectification [22].

Figure 3 indicates the functional block diagrams of the rectennas. In the conventional rectenna shown in Fig. 3 (a), antennas and rectifiers are designed independently and are connected to each other through the 50Ω interface. Recti-

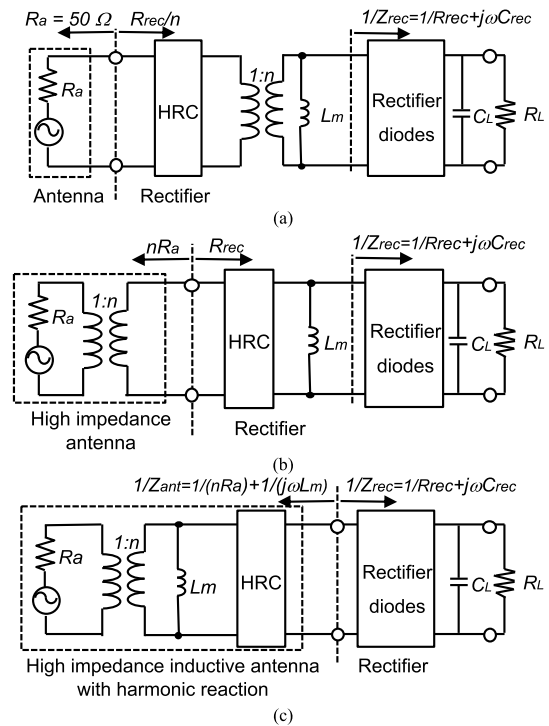


Fig. 3 Functional block diagrams of (a) a conventional rectenna, (b) a rectenna with a high impedance antenna and (c) a rectenna consisting of an inductive high impedance antenna with harmonic reaction functionality.

fier diodes can be represented as a parallel circuit with resistance R_{rec} and capacitance C_{rec} . Typically, R_{rec} is higher than 50Ω with a DC load resistance optimized for efficiency improvements. Thus, a rectenna includes the circuit functionalities of the impedance transforming to the high rectenna resistance R_{rec} , matching inductance L_m , and harmonic reaction. Implemented circuits for the above functionalities include insertion losses that result in efficiency degradation. To improve the efficiency, a high antenna impedance topology was proposed for the rectenna, as shown in Fig. 3 (b). As a high-impedance antenna, the folded dipole antenna (FDA) with an input impedance of 470Ω is employed for the rectenna, as shown in Fig. 4 [8]. For FDAs, impedances higher than $1 \text{ k}\Omega$ can be realized without radiation efficiency degradation [23]. In the developed rectifier, the functionality of the impedance transformation is realized in the FDA. The additional functionalities of the harmonic reaction and matching inductance are configured with the L-type low pass filter. The developed 2.4 GHz band bridge rectifier achieved a rectification efficiency of 81% at an input power of 29 dBm, with commercial Si SBDs (breakdown voltage: $V_{br} = 22.7 \text{ V}$; series resistance: $R_s = 7.5 \Omega$; junction capacitance at the bias voltage of 0 V: $C_{j0} = 0.7 \text{ pF}$) [8].

For further improvements, a highly functional antenna that realizes all functionalities of the RF front-end was proposed to implement a direct connection between the antenna and the rectifier diode, as shown in Fig. 3 (c). This is the proposed DoA topology implemented to improve the rectification efficiency of the high-power rectifier, as shown

in Fig. 5 [10]. An inductive high-impedance FDA and harmonic reaction feeders (HRFs) are integrated to realize all circuits' functionalities of the RF front-end. There are no lossy circuit components between the antenna and the rectifier diodes. And the parallel resonance circuit is configured with the overall rectenna. Thus, there is no standing wave at the resonance frequency. This DoA topology minimizes the loss of the interconnection and maximizes the rectification efficiency, as described in Sect. 4. The developed 2.4 GHz band rectifier achieved a rectification efficiency of 91.5% at an input power of 31 dBm, with packaged GaAs SBDs ($V_{br} = 27$ V; $R_s = 0.9 \Omega$; $C_{j0} = 0.6$ pF) [10].

Figure 6 indicates the state of the art on rectification efficiencies of rectifiers in the 2.4 GHz and 5.8 GHz bands. With the DoA topology, high rectification efficiencies can be achieved especially in 5.8 GHz band. Owing to the increment in the circuit loss, efficiency improvement is clearly

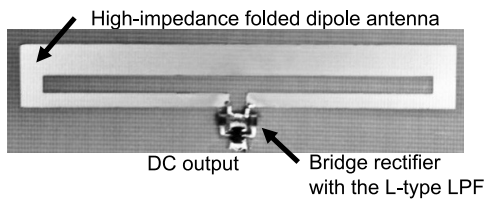


Fig. 4 Photograph of the 2.4 GHz band rectenna consisting of the high-impedance folded dipole antenna (FDA) and the bridge rectifier with the L-type LPF [8]. The FDA size is 56 mm x 8 mm.

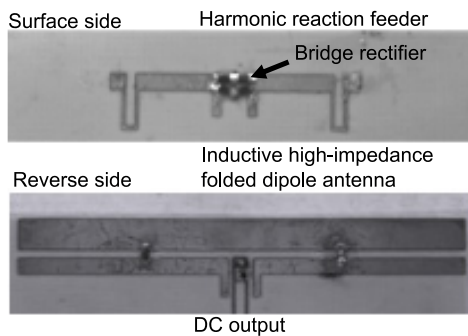


Fig. 5 Photographs of the 2.4 GHz band rectenna consisting of the bridge rectifier and the inductive high-impedance FDA with harmonic reaction feeders [10]. The FDA size is 57 mm x 7 mm.

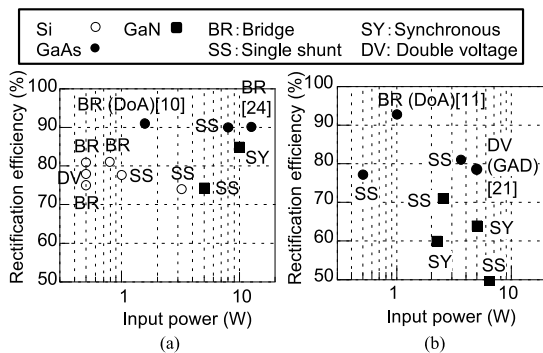


Fig. 6 Rectification efficiencies in (a) 2.4 GHz and (b) 5.8 GHz bands.

realized in the higher frequency bands.

3. Fundamental Limitation on the Rectification Efficiency of the Bridge Rectifier [24]

With the DoA topology, the circuit loss can be minimized to zero. Thus, the limitation on the rectification efficiency restricted by the rectifier diode performance can be realized with this topology. In this section, formulation of the fundamental limitation on the rectification efficiency of the bridge rectifier using the novel behavioral model is described. The derived formulas can be applied to the codesign of the antenna and rectifier.

3.1 Behavioral Model

Figure 7 indicates a functional block diagram of the bridge rectifier. The circuit functionalities of the bridge rectifier consist of the impedance transform, the harmonic reactive termination for odd-order harmonics, the matching inductance L_m , the bridge diode, and the smoothing capacitance C_L . The DC output current is outputted to the load resistance R_L . The smoothing capacitor C_L reactively terminates the even-order harmonics generated by the bridge diode.

Figure 8 illustrates the behavioral model of a bridge rectifier. The behavioral model consists of the following functional blocks:

- i) Impedance transform, which tunes the RF impedance nR_0 .
- ii) RF impedance matching with loss L_{rf} . Impedance matching was formulated with the RF impedance network of the bridge rectifier.
- iii) Rectification with efficiency η_{rec} . Rectification behavior is formulated with the rectifier current waveform obtained from the switch model of the SBD [12].

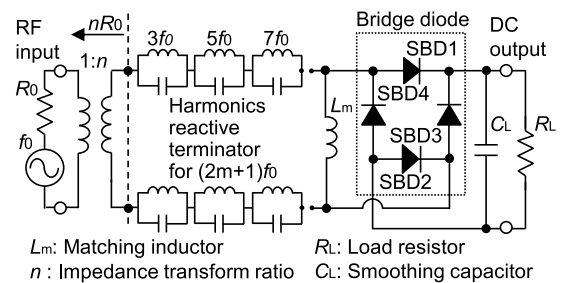


Fig. 7 Functional block diagram of the bridge rectifier (f_0 : operating frequency, $R_0 = 50 \Omega$: internal resistance of the RF power source) [24].

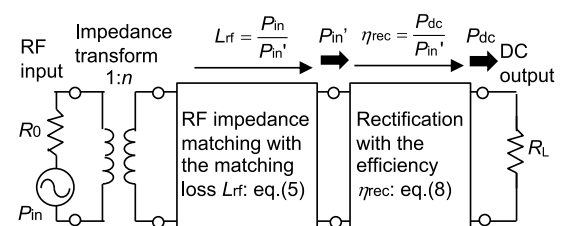


Fig. 8 Behavioral model of the bridge rectifier [24].

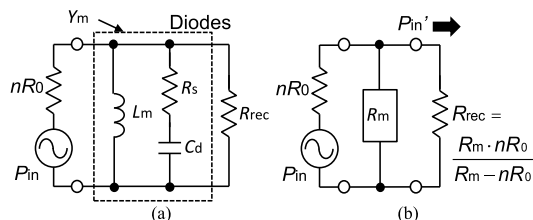


Fig. 9 (a) RF equivalent circuit of the bridge rectifier, (b) circuit in matching condition [24].

In the behavioral model, fully sufficient conditions for RF impedance matching and harmonics' recovery to DC are assumed to clarify the fundamental limitation on the rectification efficiency. Lossy components in the matching circuit are excluded from the behavioral model. Thus, the formulated rectification efficiency is only restricted by the diode performance.

In the behavioral model, the overall rectification efficiency η is defined as

$$\eta = \frac{P_{dc}}{P_{in}} = \frac{P_{in}'}{P_{in}} \cdot \frac{P_{dc}}{P_{in}'} = \frac{\eta_{rec}}{L_{rf}}, \quad L_{rf} = \frac{P_{in}}{P_{in}'}, \quad \eta_{rec} = \frac{P_{dc}}{P_{in}'}, \quad (1)$$

where P_{in} is the input power; P_{in}' is the reduced input power due to L_{rf} , and P_{dc} is the DC output power.

3.2 Formulation

Figure 9 (a) illustrates the RF equivalent circuit of the bridge rectifier. The bridge diode is represented as the RF resistances R_{rec} , R_s , and capacitance C_d . R_{rec} is the switching resistance of the bridge diode, and C_d and R_s are the parasitic components of the bridge diode. The loss of the matching inductance L_m was excluded, as mentioned. C_d is approximated as

$$C_d = C_{j0} \left[1 + |V_{dc}/(2V_t)| \right]^{-0.5} + C_p, \quad (2)$$

where V_t is the built-in voltage; C_{j0} is the zero-biased junction capacitance; C_p is the parasitic capacitance of the SBD, and V_{dc} is the output DC voltage of the bridge rectifier. This equation is a modified form of the equation for a single-shunt rectifier [25]. The matching inductor L_m is designed for conjugate matching with C_d to achieve the maximum RF power at R_{rec} . Thus, Y_m at f_0 becomes R_m as follows:

$$R_m = \frac{1 + \omega_0^2 C_d^2 \cdot R_s^2}{(\omega_0 C_d)^2 \cdot R_s} \approx \frac{1}{\omega_0^2 C_d^2 R_s}, \quad (3)$$

$$\omega_0 = 2\pi f_0 \approx \frac{1}{\sqrt{C_d L_m}}.$$

For the matching condition shown in Fig. 9 (b), R_{rec} and the power P_{in}' that is consumed at R_{rec} are given as follows:

$$R_{rec} = R_m \cdot nR_0 / (R_m - nR_0), \quad P_{in}' = [(R_m - nR_0) / R_m] P_{in}. \quad (4)$$

The matching loss L_{rf} in this RF model is given by

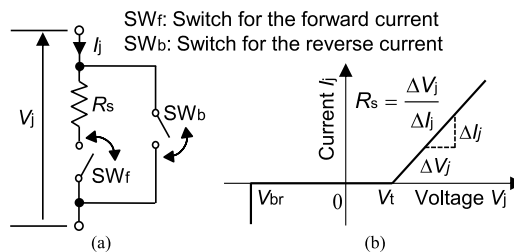


Fig. 10 Switch model of the SBD: (a) equivalent circuit, (b) DC characteristic [24].

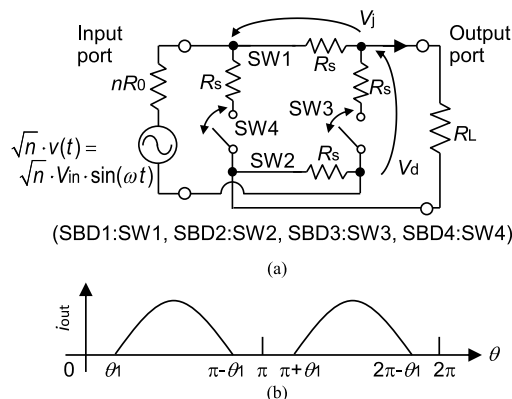


Fig. 11 Waveform of the full-wave rectification: (a) analysis model, (b) output current waveform [24].

$$L_{rf} = \frac{P_{in}}{P_{in}'} = \frac{R_m}{R_m - nR_0} = \frac{1}{1 - \omega_0^2 C_d^2 R_s \cdot nR_0}. \quad (5)$$

As indicated in Eq. (5), a higher diode capacitance C_d or RF impedance nR_0 results in a higher matching loss L_{rf} .

Next, the rectification efficiency η_{rec} is formulated using the DC characteristics of the SBD. The SBD can be represented by the switches shown in Fig. 10. The SBD is modeled as the resistor R_s and ideal switches SW_f and SW_b . Switch SW_f turns on for $V_t \leq V_j$, and switch SW_b turns on for $V_j \leq V_{br}$, as shown in Fig. 10 (b). The efficiency is analyzed with the circuit model indicated in Fig. 11 (a). The output current i_{out} indicated in Fig. 11 (b) and load resistance R_L give the overall output DC power P_{dc} including that of the harmonics.

$$P_{dc} = R_L \cdot \frac{1}{\pi} \int_{\theta_1}^{\pi - \theta_1} i_{out}^2 d\theta$$

$$= 8nR_0 R_L P_{in}' \frac{\left(\frac{\pi}{2} - \theta_1 \right) \left(1 + \frac{V_t^2}{n \cdot R_0 \cdot P_{in}'} \right) - \frac{3V_t}{\sqrt{2n \cdot R_0 \cdot P_{in}'}} \cos \theta_1}{\pi (n \cdot R_0 + 2 \cdot R_s + R_L)^2}$$

$$\theta_1 = \sin^{-1} \left\{ 2V_t / (\sqrt{n} \cdot V_{in}) \right\}, \quad \sqrt{n} \cdot V_{in} \geq 2V_t, \quad \theta = \omega t. \quad (6)$$

It is assumed that all harmonics of the output current i_{out} are converted into DC. As described, we insert the resistance R_m , which represents the matching loss L_{rf} . The RF impedance, nR_0 , of the rectifier is reduced by R_m . In general R_m has an extremely high resistance compared to that of nR_0 . The approximation $nR_0 R_m / (nR_0 + R_m) \approx nR_0$ can be used in Eq. (6). From Eq. (6), the rectification efficiency η_{rec}

is given by

$$\begin{aligned} \eta_{\text{rec}} &= P_{\text{dc}}/P_{\text{in}}' \\ &= \frac{8nR_0R_L \left(\frac{\pi}{2} - \theta_1 \right) \left(1 + \frac{V_t^2}{n \cdot R_0 \cdot P_{\text{in}}'} \right) - \frac{3V_t}{\sqrt{2n \cdot R_0 \cdot P_{\text{in}}'}} \cos \theta_1}{\pi(n \cdot R_0 + 2 \cdot R_s + R_L)^2}. \end{aligned} \quad (7)$$

At $\partial\eta_{\text{rec}}/\partial R_L = 0$, the load resistance R_L for the maximum rectification efficiency η_{rec} is given as $R_L = n \cdot R_0 + 2R_s$. With the R_L condition, η_{rec} can be expressed as:

$$\begin{aligned} \eta_{\text{rec}} &= \frac{2}{\pi} \left(1 - \frac{2R_s}{nR_0 + 2R_s} \right) \left\{ \left(\frac{\pi}{2} - \theta_1 \right) \left(1 + \frac{V_t^2}{nR_0 \cdot P_{\text{in}}'} \right) \right. \\ &\quad \left. - \frac{3V_t}{\sqrt{2n \cdot R_0 \cdot P_{\text{in}}'}} \cos \theta_1 \right\}. \end{aligned} \quad (8)$$

This formula indicates that the rectification efficiency η_{rec} can be improved with a higher RF impedance, nR_0 .

Next, the maximum input power is discussed. At first, the maximum input power P_{inmax}' of the rectification block shown in Fig. 8 is formulated. P_{inmax}' is restricted by the breakdown of the SBDs in the off state. A higher n results in a higher terminal voltage V_d of the SBDs in the off state. This results in a lower P_{inmax}' value. V_d is given by the voltage drop with the rectified DC current I_{rms} through the load resistance R_L , and the SBD in the on state. With the assumption of $\sqrt{n} \cdot V_{\text{in}} \gg 2V_t$, V_d is approximated as

$$V_d \approx \frac{\sqrt{n} \cdot (R_s + R_L)}{2\sqrt{2} \cdot R_L} \cdot V_{\text{in}} + V_t. \quad (9)$$

At the breakdown voltage $V_d = V_{\text{br}}$, P_{inmax}' under the condition of $R_L = n \cdot R_0 + 2R_s$ is derived as follows:

$$P_{\text{inmax}}' = \frac{(nR_0 + 2R_s)^2 \cdot (V_{\text{br}} - V_t)^2}{nR_0 \cdot (nR_0 + 3R_s)^2}. \quad (10)$$

With the assumptions of $nR_0 \gg R_s$ and $V_{\text{br}} \gg V_t$, P_{inmax}' can be approximated as

$$P_{\text{inmax}}' \approx \frac{V_{\text{br}}^2}{nR_0}. \quad (11)$$

This equation provides a good design guideline for the RF impedance nR_0 . A higher RF impedance, nR_0 , lowers P_{inmax}' , as discussed above.

Finally, the overall characterization of the bridge rectifier is discussed. Substituting Eq. (5) and Eq. (8) into Eq. (1), the overall rectification efficiency η is given by

$$\begin{aligned} \eta &= \eta_{\text{rec}}/L_{\text{rf}} = (1 - \omega_0^2 C_d^2 R_s \cdot nR_0) \cdot \frac{2}{\pi} \left(1 - \frac{2R_s}{nR_0 + 2R_s} \right) \\ &\quad \cdot \left[\left(\frac{\pi}{2} - \theta_1 \right) \left\{ 1 + \frac{V_t^2 (1 - \omega_0^2 C_d^2 R_s \cdot nR_0)}{nR_0 \cdot P_{\text{in}}} \right\} \right. \\ &\quad \left. - \frac{3V_t \sqrt{1 - \omega_0^2 C_d^2 R_s \cdot nR_0}}{\sqrt{2nR_0 \cdot P_{\text{in}}}} \cos \theta_1 \right]. \end{aligned} \quad (12)$$

As already discussed, the matching loss L_{rf} and rectification efficiency η_{rec} have opposite dependencies on the RF

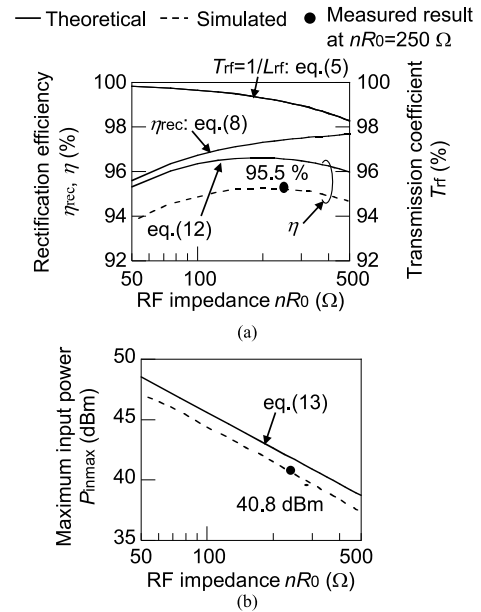


Fig. 12 Theoretical, simulated and measured values of (a) rectification efficiency and (b) maximum input power of the 2.4 GHz band 10 W rectifier [24].

impedance nR_0 , as shown in Fig. 12 (a). This indicates that there is an optimum RF impedance nR_0 that can be determined in the design procedure. With the optimum RF impedance nR_0 , the theoretical rectification efficiency is a fundamental limitation that is restricted by the diode performance. From Eq. (5) and Eq. (10), the overall maximum input power P_{inmax} is given by

$$\begin{aligned} P_{\text{inmax}} &= L_{\text{rf}} \cdot P_{\text{inmax}}' \\ &= \frac{1}{1 - \omega_0^2 C_d^2 R_s \cdot nR_0} \cdot \frac{(nR_0 + 2R_s)^2 (V_{\text{br}} - V_t)^2}{nR_0 (nR_0 + 3R_s)^2}. \end{aligned} \quad (13)$$

As shown in Fig. 12 (b), Eq. (13) represents the behavior of P_{inmax} versus the RF impedance nR_0 . The initial design of nR_0 can be established using Eq. (12) and Eq. (13).

3.3 Experimental Investigations

To confirm the effectiveness of the behavioral model and derived closed-form formulas, the theoretical, simulated, and measured values are summarized in Table 1 for the 2.4 GHz band 10 W-class rectifier [24] and the 5.8 GHz 1 W rectifier [11] described in Sect. 4. The theoretical rectification efficiencies η at the maximum input powers P_{inmax} agree well with the measured values at 2.4 and 5.8 GHz. Thus, experimental investigations confirm the effectiveness of the behavioral model and derived closed-form formulas.

4. 5.8 GHz Band Rectenna with the DoA Topology [11]

In this section, we discuss a highly efficient 5.8 GHz band

Table 1 Theoretical, simulated, and measured rectifier performances [24].

	[24]	[11]
Frequency f_0 (GHz)	2.4	5.8
Model parameters of GaAs SBDs		
V_i (V)	0.71	0.72
R_s (Ω)	0.6	1.7
C_{j0} (pF)	2.6	0.28
C_p (pF)	0.1	0.1
V_{br} (V)	61.4	25.0
RF impedance nR_0 (Ω)	250	580
Theoretical values		
η_{rec} (%)	97.4	94.2
$1/L_{rt}$ (%)	99.1	96.4
η (%)	96.6	90.8
P_{inmax} (dBm)	41.7	30.2
Simulated values by the harmonic balance method with circuit schematics of Fig. 7		
η (%)	95.2	92.2
P_{inmax} (dBm)	40.5	30
Measured values without additional circuit losses		
η (%)	95.5	92.8
P_{inmax} (dBm)	40.8	30.0

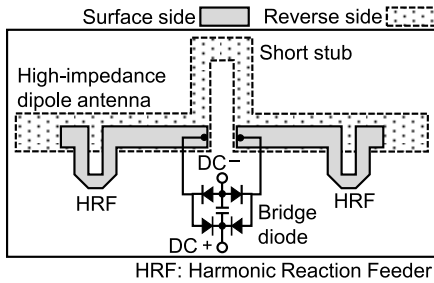


Fig. 13 Configuration of the 5.8 GHz band rectenna with the short stub connected high-impedance dipole antenna. The bridge diode is directly connected to the antenna through HRFs [11].

1 W rectenna with the DoA topology. The rectenna consists of a GaAs bridge diode and a stub connected high-impedance dipole antenna having an antenna resistance of 580 Ω .

4.1 Configuration

Figure 13 indicates the configuration of the 5.8 GHz band 1 W rectenna with the DoA topology. The highly functional antenna consists of a high-impedance dipole antenna, a short stub, and harmonic reaction feeders (HRFs). The bridge diode is directly connected to the antenna through the HRFs. On the reverse side of the substrate, there is a short stub connected high-impedance dipole antenna. On the surface side, there are HRFs, a bridge diode, and a smoothing capacitor.

Figure 14 indicates the RF equivalent circuit of the antenna. The conductance $G_a = 1/R_a$ and susceptance B_a represent the dipole antenna admittance Y_a , and B_{st} represents the short stub susceptance. The conductance G_{rec} and capacitance C_{rec} represent the RF equivalent circuits of the bridge diode. Between the short stub connected high-

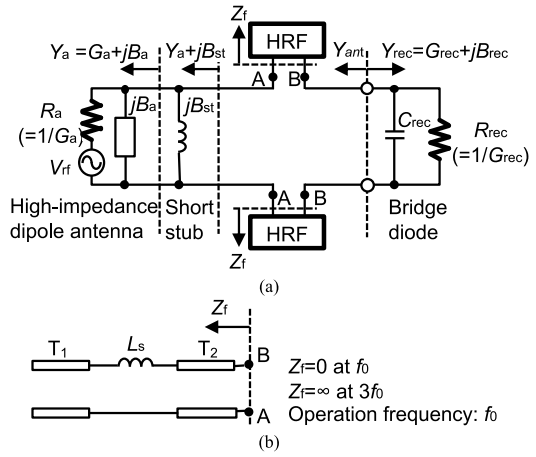


Fig. 14 RF equivalent circuit of the rectenna. (a) Overall rectenna. (b) HRF [11].

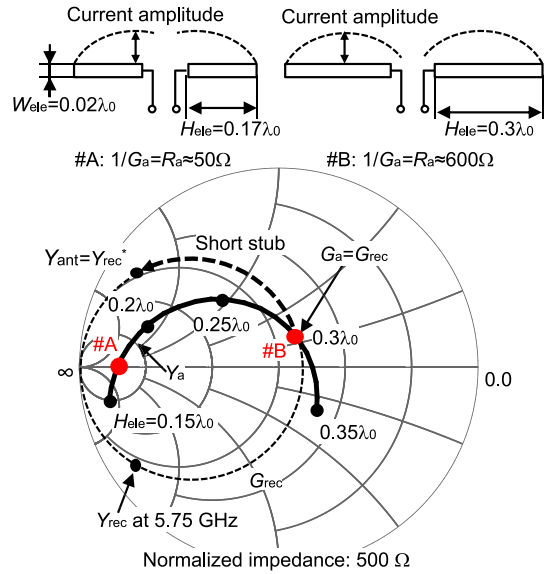


Fig. 15 Simulated dipole antenna admittance Y_a and the bridge diode's admittance Y_{rec} at 5.8 GHz band [11].

impedance dipole antenna and the bridge rectifier, there are HRFs composed of an inductor L_s and two transmission lines T_1 and T_2 , as shown in Fig. 14 (b). The HRF is designed such that the input impedance Z_f is short at f_0 and open at $3f_0$. At f_0 , the bridge diode is directly connected to the short stub connected high-impedance dipole antenna without any lossy circuit components. This indicates that $Y_{ant} = Y_a + jB_{st}$ in Fig. 14 (a). A parallel resonant circuit is configured with the antenna Y_{ant} and the bridge diode Y_{rec} , as shown in Fig. 14 (a). There is no standing wave at the resonant frequency f_0 between the antenna and the diodes. This DoA topology can minimize the interconnection loss.

Figure 15 illustrates the simulated dipole antenna admittance Y_a and the bridge diode's admittance Y_{rec} at the 5.8 GHz band. R_a increases with increasing element length H_{ele} of the dipole antenna from $0.15\lambda_0$ to $0.35\lambda_0$, where λ_0

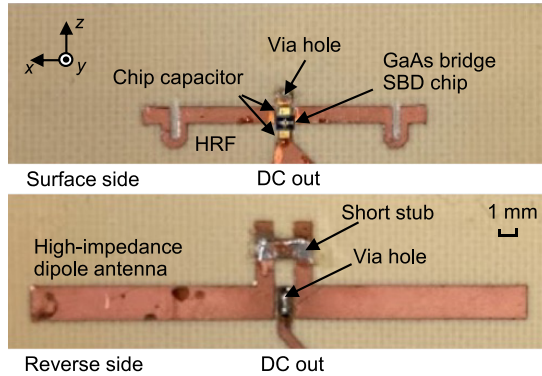


Fig. 16 Photograph of the 5.8 GHz band rectenna with the DoA topology [11].

is the wavelength at f_0 . #A in the Y_a locus on H_{ele} indicates that $R_a = 50 \Omega$ of the conventional dipole antenna with H_{ele} of $0.17\lambda_0$. #B indicates that $R_a = 580 \Omega$ of this high-impedance dipole antenna with an extended H_{ele} of $0.3\lambda_0$. The antenna conductance $G_a = 1/R_a$ is designed to be equal to the bridge diode's conductance G_{rec} . The antenna susceptance B_a is lower than that of the bridge diode's conjugate susceptance $-B_{rec}$. To obtain a conjugate matching to Y_{rec} , a short stub with susceptance B_{st} is connected in parallel to the dipole antenna. The susceptance $B_a + B_{st}$ can be aligned to be the same as $-B_{rec}$. The short stub connected high-impedance dipole antenna can realize the functionalities of the impedance transform and the impedance matching. The HRF can realize the functionalities of the third-order harmonic reaction and DC blocking.

4.2 Experimental Investigations

A photograph of the 5.8 GHz band rectenna is shown in Fig. 16. The printed circuit board employs Megtron 7 [26] and a GaAs bridge SBD chip ($V_{br} = 25$ V, $R_s = 1.7 \Omega$, $C_{j0} = 0.28$ pF). Additionally, chip capacitors of 5 pF are mounted on the surface.

The measured and simulated antenna impedances $Z_{ant} = 1/Y_{ant}$ of the short stub connected high-impedance dipole antenna with HRFs are shown in Fig. 17. The extended S-parameter method [27] is employed for the measurements.

Figure 18 indicates the measurement setup for the evaluation of the rectifier's rectification efficiency. The distance between the transmitting antenna and the rectenna is $1.25\lambda_0$, which satisfies the far-field condition. The reference antenna is used to measure the input power P_{in} to the rectifier, as shown in Fig. 18 (a). The reference antenna has the same configuration as the short stub connected high-impedance dipole antenna. The short stub is redesigned to eliminate the antenna susceptance $B_a + B_{st}$. The $\lambda_0/4$ impedance transformer is connected to the reference antenna for 50 Ω matching. The HRFs are removed from the above connection. The reference antenna had the same simulated gain as that of the rectenna. P_{in} is corrected with the loss of the $\lambda_0/4$

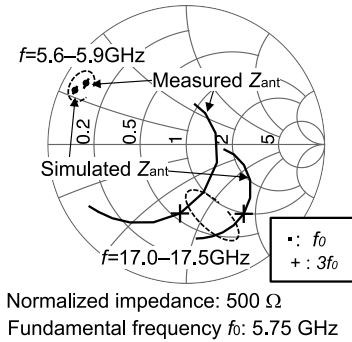


Fig. 17 Measured and simulated antenna impedance Z_{ant} of the short stub connected high-impedance dipole antenna with the HRFs [11].

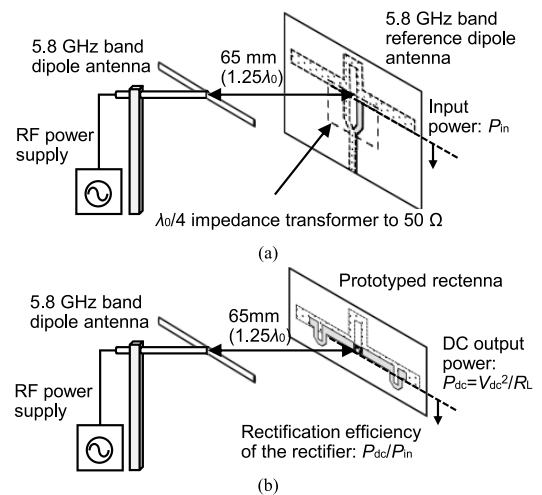


Fig. 18 Measurement setup for rectification efficiency of the rectifier: (a) input power measurement, and (b) DC output power measurement [11].

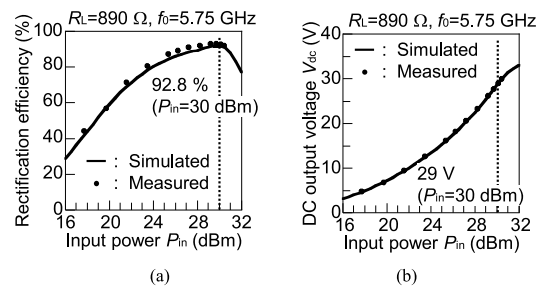


Fig. 19 Characteristics of the 5.8 GHz band bridge rectifier: (a) rectification efficiency, and (b) DC output voltage V_{dc} [11].

impedance transformer. The DC output power P_{dc} of the rectifier is measured, as shown in Fig. 18 (b). The rectenna is placed at the same position as the reference antenna. The rectification efficiency of the rectifier without antenna loss is obtained using the formula P_{dc}/P_{in} .

Figure 19 indicates the characteristics of the 5.8 GHz band bridge rectifier: (a) is the rectification efficiency, and (b) is the DC output voltage V_{dc} . The load resistance R_L is optimized to improve the rectification efficiency, and the optimized R_L is 890 Ω . The measured rectification efficiency

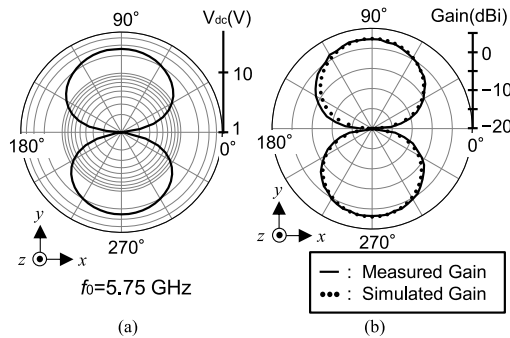


Fig. 20 Azimuth pattern of measured and simulated antenna performances of the short stub connected high-impedance dipole antenna with the HRFs: (a) measured DC output voltage of the rectenna, and (b) measured antenna gain estimated from (a) [11].

is 92.8% at an input power P_{in} of 30 dBm. Both the measured and simulated values are in good agreement, with a difference of less than 1%. The measured rectification efficiency is in good agreement with the fundamental limitation of 92.2%, as shown in Table 1.

Figure 20 indicates the azimuth pattern of the measured and simulated antenna performances of the short stub connected high-impedance dipole antenna with HRFs. The measurement setup is the same as that shown in Fig. 18 (b). The antenna gain is obtained from the difference in the input power between the standard dipole antenna and the rectenna. For the input power measurement, the standard dipole antenna is placed at the same position as that of the rectenna, as shown in Fig. 18 (b). The input power of the rectenna is estimated from the measured V_{dc} versus input power P_{in} , as shown in Fig. 19 (b). The measured antenna gain of 2.3 dBi at an azimuth of 90° is lower than the simulated one of 2.4 dBi. The measured antenna radiation efficiency can be estimated from the gain difference of 0.1 dB, under the assumption of the same antenna radiation patterns in the simulation and measurement. The measured antenna radiation efficiency of 96.9% is estimated from the simulated value of 99.2% and includes losses due to the circuit functionalities and interconnection between the antenna and the bridge diode. The proposed DoA topology, which is the direct connection between the proposed antenna and the bridge diode, eliminates the additional loss due to lossy circuit components under the standing wave by interconnection.

Thus, the rectifier in our study achieved the highest rectification efficiency of 92.8% among the 5.8 GHz band rectifiers.

Based on the above discussion, the effectiveness of the proposed DoA topology can be confirmed via experimental investigations.

5. Conclusion

In this paper, high-power rectifiers and rectennas were discussed for highly efficient high-power rectification in MPT systems. Topologies of reported rectifiers and rectennas were summarized, and a rectenna with the DoA topology

was proposed to minimize circuit losses and achieve efficiency limitations. The formula for the rectification efficiency was derived to clarify the fundamental limitations. The developed 5.8 GHz band rectenna with the proposed DoA topology achieved a rectification efficiency of 92.8% at an input power of 1 W, which is close to the fundamental limitation calculated with the derived formula. The effectiveness of the proposed DoA topology was confirmed with experimental investigations.

Acknowledgments

This work is supported by i) the Council for Science, Technology, and Innovation (CSTI), Cross-ministerial Strategic Innovation Promotion Program (SIP), “Energy system of an Internet of Energy (IoE) society” (founding agency: JST), and ii) the National Institute of Information and Communications Technology (NICT) of Japan.

References

- [1] W.C. Brown, “The history of power transmission by radio waves,” *IEEE Trans. Microw. Theory Techn.*, vol.32, no.9, pp.1230–1242, Sept. 1984.
- [2] N. Shinohara and H. Matsumoto, “Experimental study of large rectenna array for microwave energy transmission,” *IEEE Trans. Microw. Theory Techn.*, vol.46, no.3, pp.261–268, March 1998.
- [3] H. Matsumoto, “Research on solar power satellites and microwave power transmission in Japan,” *IEEE Microw. Mag.*, vol.3, no.4, pp.36–45, Dec. 2002.
- [4] J.O. McSpadden and J.C. Mankins, “Space solar power programs and microwave power transmission technology,” *IEEE Microw. Mag.*, vol.3, no.4, pp.46–57, Dec. 2002.
- [5] Y. Fujino, “A dual polarization microwave power transmission system for microwave propelled airship experiment,” *Proc. Int. Symp. on Antennas and Propag. (ISAP)*, pp.393–396, Chiba, Japan, Sept. 2016.
- [6] J.L. Gómez-Tornero, M. Poveda-García, R. Guzmán-Quirós, and J.C. Sánchez-Arnause, “Design of Ku-band wireless power transfer system to empower light drones,” *Proc. Wireless Power Transfer Conference (WPTC)*, Aveiro, Portugal, May 2016.
- [7] T. Saen, K. Itoh, S. Betsudan, S. Makino, T. Hirota, K. Noguchi, and M. Shimosawa, “Fundamentals of the bridge RF rectifier with an impedance transformer,” *Proc. IEEE MTT-S Int. Microw. Workshop Series on Innovative Wireless Power Transmission: Technologies, Systems, and Applications*, pp.255–258, Kyoto, Japan, May 2011.
- [8] M. Ito, K. Hosodani, K. Itoh, S. Betsudan, S. Makino, T. Hirota, K. Noguchi, and E. Taniguchi, “High efficient bridge rectifiers 100 MHz and 2.4 GHz bands,” *Proc. IEEE Wireless Power Transfer Conf. (WPTC)*, pp.64–67, Jeju, Korea, June 2014.
- [9] A. Hirono, N. Sakai, and K. Itoh, “High efficient 2.4GHz band high power rectenna with the direct matching topology,” *Proc. IEEE Asia-Pacific Microw. Conf. (APMC)*, Singapore, pp.1268–1270, Singapore, Dec. 2019.
- [10] A. Mugitani, A. Hirono, N. Sakai, and K. Itoh, “High efficient 2.4 GHz band rectenna with the harmonic reaction FDA,” *Proc. IEEE Wireless Power Transfer Conf. (WPTC)*, pp.191–193, Seoul, Korea, Nov. 2020.
- [11] N. Sakai, K. Noguchi, and K. Itoh, “A 5.8 GHz band highly efficient 1 w rectenna with short stub connected high-impedance dipole antenna,” *IEEE Trans. Microw. Theory Techn.*, vol.69, no.7, pp.3558–3566, July 2021.
- [12] J. Hashimoto, K. Itoh, M. Shimosawa, and K. Mizuno, “Fundamental limitations on the output power and the third-order distortion of

balanced mixers and even harmonic mixers,” *IEEE Trans. Microw. Theory Techn.*, vol.64, no.9, pp.2853–2862, Sept. 2016.

[13] K. Kawakami, M. Shimozawa, H. Ikematsu, K. Itoh, Y. Isota, and O. Ishida, “A millimeter-wave broadband monolithic even harmonic image rejection mixer,” *IEEE MTT-S Int. Microw. Symp. Dig.*, pp.1443–1446, Baltimore, MD, USA, June 1998.

[14] W.C. Brown, “Optimization of the efficiency and other properties of the rectenna element,” *IEEE MTT-S Int. Microw. Symp. Dig.*, pp.142–144, Cherry Hill, NJ, USA, June 1976.

[15] A. Noda and H. Shinoda, “Compact class-F RF-DC converter with antisymmetric dual-diode configuration,” *IEEE MTT-S Int. Microw. Symp. Dig.*, Montreal, QC, Canada, June 2012.

[16] S.A. Rotenberg, S.K. Podilchak, P.D. Hilario Re, C. Mateo-Segura, G. Goussetis, and J. Lee, “Efficient rectifier for wireless power transmission systems,” *IEEE Trans. Microw. Theory Techn.*, vol.68, no.5, pp.1921–1932, May 2020.

[17] M. Roberg, T. Reveyard, I. Ramos, E.A. Falkenstein, and Z. Popović, “High-efficiency harmonically terminated diode and transistor rectifiers,” *IEEE Trans. Microw. Theory Techn.*, vol.60, no.12, pp.4043–4052, Dec. 2012.

[18] R. Ishikawa and K. Honjo, “High-efficiency DC-to-RF/RF-to-DC interconversion switching module at C-Band,” *Proc. European Microw. Conf. (EuMC)*, pp.295–298, Paris, France, Sept. 2015.

[19] T. Umeda, H. Yoshida, S. Sekine, Y. Fujita, T. Suzuki, and S. Otaka, “A 950-MHz rectifier circuit for sensor network tags with 10-m distance,” *IEEE J. Solid-State Circuits*, vol.41, no.1, pp.35–41, Jan. 2006.

[20] S. Yanagihara, S. Tschimoto, K. Itoh, K. Kawasaki, T. Yao, and M. Tsuru, “The 2.4 GHz band SOI-CMOS bridge rectifier IC,” *Proc. IEEE Wireless Power Transfer Conference (WPTC)*, Taipei, Taiwan, May 2017.

[21] K. Itoh and N. Sakai, “Highly efficient high-power rectenna techniques,” *Proc. IEEE International Symposium on Radio-Frequency Integration Technology (RFIT)*, Hualien, Taiwan, Aug. 2021.

[22] H. Takahashi, Y. Ando, Y. Tsuchiya, A. Wakejima, H. Hayashi, E. Yagyu, K. Kikkawa, N. Sakai, K. Itoh, and J. Suda, “Electrical characteristics of gated-anode diodes based on normally-off GaN HEMT structures for rectenna applications,” *Electron. Lett.*, vol.57, no.21, pp.810–812, July 2021.

[23] H. Miyagoshi, K. Noguchi, K. Itoh, and J. Ida, “High-impedance wideband folded dipole antenna for energy harvesting applications,” *Proc. Int. Symp. on Antennas and Propag. (ISAP)*, pp.601–602, Kaohsiung, Taiwan, Dec. 2014.

[24] K. Kikkawa, T. Saen, N. Sakai, and K. Itoh, “A 2.4-GHz 10-W class bridge rectifier and its efficiency analysis with the behavioral model,” *IEEE Trans. Microw. Theory Techn.*, vol.70, no.3, pp.1994–2001, March 2022.

[25] J.O. McSpadden, L. Fan, and K. Chang, “Design and experiments of a high-conversion-efficiency 5.8-GHz rectenna,” *IEEE Trans. Microw. Theory Techn.*, vol.46, no.12, pp.2053–2060, Dec. 1998.

[26] “High speed, low loss multi-layer materials MEGTRON7(G) data sheet,” Panasonic Corp., no.20042028, April 2020. [Online]: [https://industrial.panasonic.com/content/data/EM/PDF/ipcdatasheet_R-5785\(G\).pdf](https://industrial.panasonic.com/content/data/EM/PDF/ipcdatasheet_R-5785(G).pdf).

[27] T. Fukasawa, T. Yanagi, H. Miyashita, and Y. Konishi, “Extended S-Parameter method including radiation pattern measurements of an antenna,” *IEEE Trans. Antennas Propag.*, vol.60, no.12, pp.5645–5653, Dec. 2012.



a member of the IEICE and a fellow of the IEEE.

Kenji Itoh received his B.S. degree in Electrical Engineering from Doshisha University, Kyoto, Japan, in 1983 and a Ph.D. degree in electrical engineering from Tohoku University, Miyagi, Japan, in 1997. He joined Mitsubishi Electric Corporation in 1983. Since 2009, he has been a professor at the Department of Electronics, Kanazawa Institute of Technology, Ishikawa, Japan. His research interests include microwave and millimeter wave circuits, such as mixers, oscillators and rectennas. He is



a member of IEICE and IEEE. His research interests include microwave technologies for microwave power transfer and RF energy harvesting. He is a member of IEICE and IEEE.

Naoki Sakai received his B.E. degree in Information Engineering from Toyohashi University of Technology, Aichi, Japan, in 2006 and Dr. Eng. degree in Electronic and Information Engineering from Toyohashi University of Technology in 2013. From 2014 to 2019, he was an assistant professor in Toyohashi University of Technology. Since 2019, he has been with the Center for Electric, Optic, and Energy Applications at Kanazawa Institute of Technology, where he is working as a researcher. He is a



where currently he is a professor. His research interests include on small antennas, such as helical, meander-line, dielectric resonator, and microstrip antennas. He is a member of IEICE and IEEE.

Keisuke Noguchi received his B.E. and Dr. Eng. degrees in Electrical Engineering from the Kanazawa Institute of Technology, Ishikawa, Japan, in 1990 and 1998, respectively, and the M.E. degree in Electrical Engineering from Tohoku University, Sendai, Japan, in 1992. From 1992 to 1995, he worked at the Central Research Laboratory of Hitachi, Ltd. Since 1995, he has been with the Department of Electronics, Information and Communication Engineering at Kanazawa Institute of Technology,